Journal of
Materials Chemistry B

Accepted Manuscript

This article can be cited before page numbers have been issued, to do this please use: R. Motaghed Mazhabi, L. Ge, H. Jiang and X. Wang, *J. Mater. Chem. B*, 2018, DOI: 10.1039/C8TB01067F.

ROYAL SOCIETY OF CHEMISTRY

rsc.li/materials-b

A Label-Free Aptamer Based Cytosensor for Specific Cervical Cancer HeLa Cell Recognition through g-C_3N_4-AgI/ITO Photoelectrode

Robabeh Motaghed Mazhabi, Liqin Ge, Hui Jiang, Xuemei Wang*

State Key Laboratory of Bioelectronics (Chien-Shiung Wu Laboratory), School of Biological Science and Medical Engineering, Southeast University, Nanjing 210096, China

*Corresponding Author:

E-mail: xuewang@seu.edu.cn. Tel/Fax: +86-25-83792177

View Article Online
DOI: 10.1039/C8TB01067F

ABSTRACT

Facile and efficient detection of cancer cells at the early phases of a disease is one of the main challenges in the cancer diagnostics. It is found that photoactive materials and bio-recognition elements are two key factors for a promising photoelectrochemical (PEC) biosensor for cancer cell detection which could play a significant role for realizing the cancer early diagnostics with high sensitivity and selectivity. In this study, we designed a novel label-free PEC aptamer based cytosensor for the specific detection of cancer cells like Hela cells by using water-dispersible g-C_3N_4-AgI nanocomposites as visible light-sensitive material and anti-CEM/PTK7 aptamer as the bio-recognition element. It is observed that when a suitable amount of AgI nanoparticles were doped in the two-dimensional graphite-like carbon nitride nano-sheets (g-C_3N_4 NSs), the visible light photocurrent response could be significantly improved. The PEC response of the as-prepared biosensor based on g-C_3N_4-AgI/ITO photoelectrode was linearly proportional to the relevant cancer cells like Hela cells in the concentration ranging from 10 to 10^6 cells/mL with a limit of detection of 5 cells/mL. In addition, the g-C_3N_4-AgI/ITO photoelectrode and the fabricated cytosensor exhibit long-term stability, good reproducibility, excellent selectivity, and high sensitivity, demonstrating the successful conjugation of g-C_3N_4-AgI NSs with aptamer and target cancer cells in the high performance PEC cytosensor.

KEYWORDS: g-C_3N_4-AgI nanocomposites; photoelectrochemistry; aptamer; Hela, cancer cells; cytosensor

1. Introduction

While cancer has become one of the main causes of death worldwide nowadays, more interest has been concentrated on the early diagnosing and screening of cancer cells in recent years. Strategies that enable early detection of cancer cells with high selectivity and sensitivity are highly desired in cancer diagnostics and therapy.[1-3] Measuring the specific cellular level within the blood can help the doctor to evaluate the patient's reaction to treatment or predict the probability of developing a specific disease.[4] However, because of costly instruments, long time analytical process, and complicated operations, traditional analysis techniques such as polymerase chain reaction (PCR)[5], immunohistochemistry[6] and flow cytometer[7] do not meet the requirement of point-of-care (POC) diagnostics.[8] Thus, the development of a simple diagnostic tool for specific and ultrasensitive detection of cancer cells at low cost is necessary.[4] Because of the advantages of simple instrumentation, low cost, rapid analysis, and portable instruments, the photoelectrochemical (PEC) sensors have attracted increasing research interest in recent years.[9] It is a newly emerging and promising analytical technique with desirable advantages, such as lower background signal and higher sensitivity, which is helpful and essential to be explored as an effective means for disease early diagnosis.[10-13] Typically in a PEC sensing system, a photoelectrode is employed to convert photo-irradiation to electrical signal, which is proportional to the concentration of the analytical substrates.[12, 14] Since the photoactive materials and relevant photoelectrodes play an important role in PEC detection, graphite-like carbon nitride (g-C_3N_4) has recently received much attention owing to its interesting photo-catalytic properties and special nanostructure such as a layer spacing about 3.3 nm, a proper HOMO-LUMO energy band gap of about 2.7 eV, weak van der Waals forces between C−N layers, and delocalized conduction and valence bands, which are conducive to the charge transport.[15] In addition, g-C_3N_4 is an inexpensive. non-toxic, abundant and stable material with an easy controllable surface for

film making.[16] So, as a chemically and thermally stable semiconductor, g-C_3N_4 has a widely application in the fields of photoelectronic materials,[17, 18] sensors,[19, 20] catalysis,[21-23] degradation,[24, 25] and so forth. Due to its macroscopic size and low photo-response, the bulk g-C_3N_4 is not suitable for sensor fabrication. Recently much attention has been focused on the application of ultrathin two-dimensional (2D) g-C_3N_4 nanosheets (NSs) for their unique optical, electronic, and biocompatible properties, which made them more suitable for practical applications regarding to the bulk materials.[26] Owing to high water-dispersibility potential of g-C_3N_4, single or several layered g-C_3N_4 nanosheets (NSs) has been further explored for their high fluorescent quantum yield, strong electrochemiluminescence (ECL) activity, easy film making, photoelectrode fabrication, good biocompatibility, and improved photo-catalytic property.[27, 28]

Although g-C_3N_4 NSs with high PEC properties can be used as a desirable sensing system for biological and environmental monitoring, the PEC activity of pure g-C_3N_4 NSs is highly conditional to recombination rate of photogenerated electron-hole pairs. Therefore, combining g-C_3N_4 with other different kinds of materials could be an effective solution to prevent electron- hole recombination and boost the PEC property of the g-C_3N_4.[29]

Silver halides (AgX, X = Br, I) are well-known as important photoactive materials which have excellent photo-catalytic property and extensive application in photography.[30-32] Although AgX is strong visible light photons absorbent for electron–hole pairs generation, pure AgBr or AgI are not stable enough under visible light as they easily be decomposed, which hampers their applications. Fortunately, well dispersing of AgX on the supporting materials, such as ZnO,[33] TiO_2,[32] WO_3,[34] $BiPO_4$,[35] Fe_3O_4 nanoparticle,[36] Ag_3PO_4,[37] H_2WO_4,[38] zeolite,[30, 39] etc., can prevent their decomposition, and thus help to maintain their stability and enhance the photo-catalytic activity.[31]

In order to attain a particular photoelectrical response to biomaterials, some bio-recognition elements such as DNA,[40, 41] molecularly imprinted polymers,[42] antibodies,[43, 44] enzymes,[45] and aptamers[46, 47] have been coupled on photoelectrodes surface in PEC biosensors. Among these, aptamers, the artificial oligonucleotides with high specific binding ability comparable with antibody, can bind some specific analytes, such as organic and in-organic chemicals, proteins, and cells.[48, 49] Furthermore, comparing antibodies, aptamers propose preferable advantages, such as smaller size, higher stability, lower cost, easier modification, nontoxicity, and lack of immunogenicity.[50, 51] Additionally, aptamers can be created by using cell-Selex with high affinity to the special cancer cells as targets[52] and these efforts have brought a great opportunity to develop aptamer-based biosensors for early cancer diagnosis.[53] A lot of progress has been made in the fabrication of various aptamer-based biosensors, including fluorescent sensor, colorimetric sensor,[54] electrochemical sensor,[55] cantilever sensor,[56] PEC sensor[57] and fluorometric sensor.[58] However, most of these biosensors need more time consumption and costly surface confinement of aptamers *via* covalent bonding,[59] avidin−biotin interaction,[60] or DNA−compound interactions.[61] Among these, the PEC label-free biosensor can combine the advantages of PEC method and label-free bioassay, avoiding the time consuming process of labeling the bio-recognition elements such as antibody, aptamer, cell or antigen with markers, making its construction more facile, cheaper and faster. Accordingly, the concentrations of the antigens or cells are directly measured through the hindrance-induced photocurrent reduction resulting from the specific reaction between bio-recognition elements, such as antibody or aptamer as a receptor molecule, which has already been immobilized on one side of the relevant sensor surface. [62]

On the basis of the above considerations, coupling of g-C_3N_4 as a supporting material with AgX was further explored in this contribution to facilitate the photoelectrochemical response of the g-C_3N_4 and the stability of AgX. In our previous paper, the potassium

ferrocyanide effect in buffer solution as an electron donor for photocurrent enhancement of g-C_3N_4 modified Indium tin oxide (ITO) photoelectrode was reported.[63] In the present work, this study was further evaluated for g-C_3N_4-AgX (X = Cl, Br)/ITO photoelectrodes and the photocurrent enhancement due to potassium ferrocyanide effects were compared for each photoelectrodes. The results of the comparisons in buffer solution and also in the present of potassium ferrocyanide showed that the water-dispersible AgI-g-C_3N_4 could be readily utilized for the construction of a label-free PEC aptamer based cytosensor for specific cancer cell detection, where the as-prepared g-C_3N_4-AgI NSs modified Indium tin oxide (ITO) photoelectrode could be facilely immobilized by using low-cost and label-free anti-SEM/PTK7 DNA aptamer.

2. Experimental

Materials and Reagents

ITO slices were purchased from South China of Hunan science and technology (Shenzhen) Co., Ltd. (sheet resistance <6 ohm sq−1). Potassium hexacyanoferrate (II) trihydrate was bought from Shanghai chemical reagent Co. Ltd. The anti-SEM/PTK7 oligoss DNA aptamer with the sequence;

(5’-TAAAATACCAGCTTATTCAATTAGTCACACTTAGAGTTCTAGCTGCTGCGC

C GCCGGGAAAATACTGTACGGATAGATAGTAAGTGCAATCT-3’)

was provided from Sangon biotech Co., Ltd. (Shanghai) and the aptamer powder was diluted by applying phosphate buffer solution (PBS, pH 7.4) and then the prepared solution was kept at -20.°C. All Analytical grade materials were applied for all the experiments and used as received. Deionized water (18 MΩ cm-1, Milli-Q, Millipore) was consumed for preparing all the solutions.

View Article Online
DOI: 10.1039/C8TB01067F

Instrumentation

PEC measurements were performed using a CHI660C electrochemical workstation (CH Instruments, Austin, TX) in conjugate with a 150 W Xe lamp (Beijing NBeT Co., Ltd. China) for visible light illumination. Scanning electron microscopy (SEM) images were acquired by a Hitachi S-4800 (Hitachi, Tokyo, Japan). Transmission electron microscopy (TEM) images were obtained on a JEM-2100 TEM (JEOL, Tokyo, Japan) with an accelerating voltage of 200 kV. The energy dispersives spectroscopy (EDS) spectrum was generated with ZEISS ultraplus (Germany) at an accelerating voltage of 20 kV. Electrochemical impedance spectroscopy (EIS) experiments were carried out by using an Autolab PGSTAT302N system (Eco Chemie, Netherlands), with frequency ranging from 0.01 to 105 Hz and amplitude of 10 mV. The UV–Vis absorption spectra were obtained through a Biomate 3S spectrophotometer (Thermo Co. Ltd., US). Fluorescence (FL) measurements were performed by using a RF-5301PC fluoremeter (Shimadzu, Tokyo, Japan). The Fourier transform infrared spectra (FTIR) of the samples were recorded by using Bruker tensor 27 spectrometer (Germany). The crystalline phases of g-C_3N_4-AgX hybrid materials were analyzed by X-ray diffraction (XRD) by Bruker D500 diffractometer.

Preparation of bulk g-C_3N_4

According to the previously reported procedure,[15] the bulk g-C_3N_4 was syntesized by polymerizing the melamine molecules under a high temperature condition. In details, using the heating and cooling procedure with a gradient rate of about 3 ^oC /min for 2 h, the melamine molecules was heated at 600 ^oC under air condition. The obtained yellow product was milled in a mortar to g-C_3N_4 powder.

Preparation of g-C_3N_4-AgBr Nanocomposite

g-C_3N_4-AgBr nanocomposite was synthesized as per the reported procedure with a little modifications.[64] Firstly, 150 mg of g-C_3N_4 was added into 20 mL ethanol and the suspension was sonicated for 2 h. Then, 50 mL aqueous solution of hexadecyltrimethyl ammonium bromide (CTAB) 0.1 M was added into the resulting suspension under the continuous magnetic stirring for 10 h. Afterwards, 50 mL aqueous solution of 0.1 M $AgNO_3$ was gradually added to the above mixture under stirring condition. After the addition of $AgNO_3$ aqueous solution, the obtained suspension was stirred for 6 h. Finally, the ultimate product was filtered, followed by three times washing with deionized water and absolute ethanol, respectively, dried at 333 K.

Preparation of g-C_3N_4-AgI Nanocomposite

g-C_3N_4-AgI nanocomposite was obtained as per the procedure given for the synthesis of g-C_3N_4-AgBr, but here instead of using CTAB aqueous solution, $AgNO_3$ 0.1 M solution was applied into the suspension.

Preparation of g-C_3N_4-AgX Nanosheet Solution

The g-C_3N_4-AgX NSs solution was prepared as per the reported protocol.[15] Preparation of a suitable g-C_3N_4-AgX NSs solution was performed with the help of exfoliation process of the as-prepared bulk g-C_3N_4-AgX in water. In details, 100 mg of bulk g-C_3N_4-AgX powder was added to 100 mL water and sonicated for 16 hours. The obtained suspension was centrifuged at about 500 rpm to remove the remaining unexfoliated parts and the large-area NSs of g-C_3N_4-AgX before using for photoelectrochemical sensor application.

View Article Online
DOI: 10.1039/C8TB01067F

Fabrication of the PEC Aptamer based Sensor

Prior to the electrode modification, ITO electrodes were treated to increase their hydrophilic properties. To do this, ITO electrodes were cleaned in a hot solution of 1 M KOH dissolved in 2-propanol for 15 min under the process of sonication, washed with ultrapure water, and dried at 70 °C for 2 h. The PEC sensor was fabricated by dropping a certain amount of homogeneous suspension of g-C_3N_4-AgI nanosheets (40 μL) on a specified part of ITO slice with a geometric area of (0.7 × 0.7 cm^2). The film was firmed in the air and ready to be used as a photoelectrode for immobilizing bio-recognition elements for cancer cell detection propose. Then 30 μL (100 nM) sga16 (anti-SEM/PTK7 oligoss DNA) aptamer solution was dropped on g-C_3N_4-AgI /ITO electrode surface for incubation purpose and preserved for 30 min at ambient temperature in a humid chamber to prevent water evaporation. Then the electrode was rinsed with PBS for several times and prepared for cell detection step.

Cell Culture and Incubation on the Aptamer based Modified Electrode

The human cervical cancer (HeLa) cells were provided from Shanghai cell resource institute for biological sciences. The cells were cultured as reported previously[7] by using Dulbecco's modified Eagle's medium (DMEM) (Hyclone) which has completed as a culture media with 100 μg/mL streptomycin (Hyclone), 100 U/mL penicillin (Hyclone) and 10% fetal bovine serum (Hyclone) in an incubator with humidified air (relative humidity of 95%) with 5% CO_2 at 37.0 °C .Trypsin (0.1%, m/v) was applied to detach the cells from each other as well as from petri dish and remove after ~10 min of treatment. Afterwards, 2 mL of pre-warmed complete media was added to petri dish to inactivate the trypsin and pipetted over the cell layer surface for several times to ensure recovery of >95% of cells. The cells suspension were transferred to a tube and gently centrifuged at 1000 rpm for 5-10 min. After removing the supernatant liquid, the cells were washed 3 times with sterile PBS (pH 7.4) to gain pure cells.

View Article Online
DOI: 10.1039/C8TB01067F

Then the cell suspension was prepared by adding 2 mL of sterile PBS to the collected cells precipitate and its density was determinate by means of hemocytometer. For analyzing step the cell suspension was diluted to different cell concentration with sterile PBS.

The incubation step of aptamer-modified electrodes was performed with different concentration of Hela cells suspension for ~15 - 20 min to obtain an immobilized cell-sensor (ITO/g-C_3N_4-AgI/Aptamer/Cell). To remove nonspecifically adsorbed cells the prepared electrodes were rinsed by using PBS with pH 7.4.

3. Results and Discussion

Materials Characterization

Detailed structural information and typical morphological differences in the texture of bulk g-C_3N_4, g-C_3N_4 NSs, g-C_3N_4–AgBr NSs, g-C_3N_4–AgI NSs were obtained by scanning electron microscopy (SEM) while investigation of the AgI and AgBr particles size in the structure of g-C_3N_4 nanosheets was carried out by Transmission electron microscopy (TEM). Figure 1 exhibits the SEM and TEM images of bulk g-C_3N_4 and the bare g-C_3N_4 NSs as well as g-C_3N_4-AgBr NSs. The differences between the SEM images of the bulk and NSs from g-C_3N_4 reveal water-exfoliation effect on changing the bulk g-C_3N_4 structure to ultrathin g-C_3N_4 NSs. In this Figure, bare g-C_3N_4 NSs displays both 2D and transparent structure compared to the bulk g-C_3N_4. Similar to the bare g-C_3N_4 NSs, g-C_3N_4-AgBr NSs also exhibits 2D and transparent structure. One can see from the TEM image of C_3N_4-AgBr NSs (Figure 1E) that most of the AgBr nanoparticles (50 nm in diameter) well combined with g-C_3N_4 NSs and are uniformly distributed in the structure of g-C_3N_4 NSs.

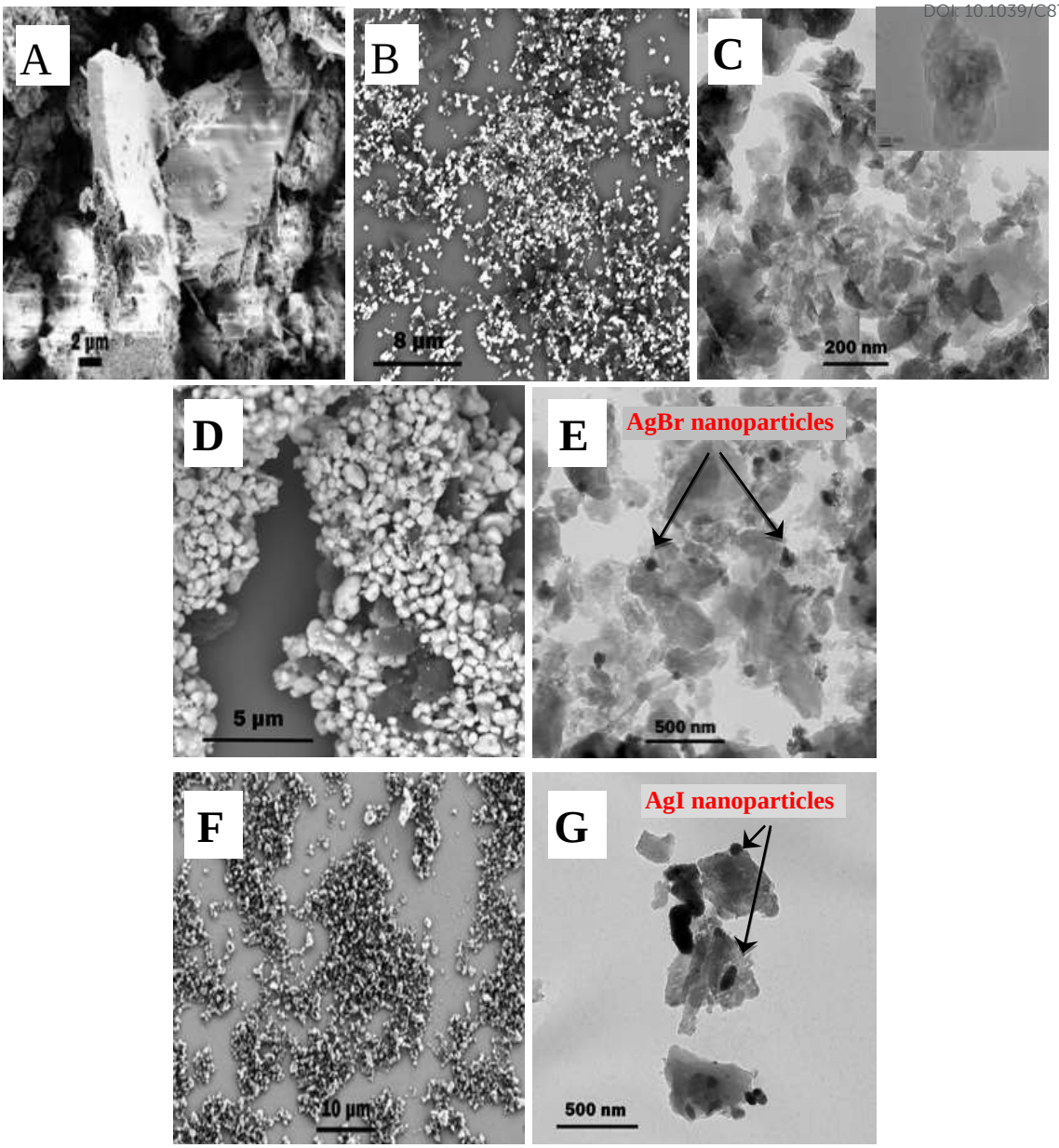

Figure 1. SEM images of **(A)** bulk g-C_3N_4 and **(B)** g-C_3N_4 NSs. TEM image of **(C)** g-C_3N_4 NSs. **(D)** SEM and **(E)** TEM images of g-C_3N_4-AgBr NSs. **(F)** SEM and **(G)** TEM images of g-C_3N_4-AgI NSs.

Similarly, Figure 1F and 1G represents the SEM and TEM images of g-C_3N_4-AgI NSs. SEM image clearly shows 2D and transparent structure of g-C_3N_4-AgI NSs and also displays uniform distribution of AgI nanoparticles with a diameter of almost 70 nm in the g-C_3N_4 NSs matrix. It is noted from Figure 1E and 1G that the nanoparticles of AgBr and AgI are distributed in the surface of g-C_3N_4 in a fine composition, which would be advantageous for

the photogenerated carrier transfer and photoactivity improvement. The composition and content of the prepared g-C_3N_4-AgI were obtained by EDS which weight and atomic ratio of C, N, Ag, and I elements are clearly indicated in Figure S2 and Table S1. The composition and content of the as-prepared g-C_3N_4-AgI were obtained by energy dispersives spectroscopy (EDS) (Figure S2) which clearly indicates the weight and atomic ratio of C, N, Ag, and I elements that are shown in Table S1. The structure of the as-prepared g-C_3N_4-AgI composite was characterized by XRD. The results shown in Figure S3a indicate that the characteristic peak of g-C_3N_4 around 27.4◦ could be clearly identified because of the pure g-C_3N_4 sample which is due to the stacking of the conjugated aromatic system.[31] As it can be seen in Figure S3b after doping of AgI nanoparticles in the structure of g-C_3N_4, the diffraction peaks at 2θ = 22.3◦, 27.3◦, 39.2◦ and 46.2◦ were observed, indicating the crystal phase of the AgI nanoparticles.

Figure S4 shows a comparison of the FTIR spectra of the pure g-C_3N_4 (Figure S4a) and g-C_3N_4-AgI (Figure S4b) composites. In the case of pure g-C_3N_4, the strong bands in the 807 cm^{-1} and 1200 – 1650 cm^{-1} region were observed, with the peaks at 1242, 1322, 1412, 1563, and 1634 cm^{-1}, which corresponded to the typical stretching vibration modes of C=N and C─N heterocycles.[31] It could also be clearly seen that the main characteristic peaks of g-C_3N_4 appeared in all g-C_3N_4- AgI photocatalysts. In the case of the g-C_3N_4-AgI composites, the characteristic peaks of g-C_3N_4 have almost no shift (red shift or blue shift) after the introduction of AgI nanoparticles. This result indicated that in the g-C_3N_4-AgI system, there was no covalent bond between g-C_3N_4 and AgI nanoparticles.

View Article Online
DOI: 10.1039/C8TB01067F

UV−Visible Absorption, Electrochemical Impendence and Florescence Spectroscopy Characterizations

In PEC determinations, it is essential to identify the best absorption area for the photoactive materials in order to choose an appropriate illuminating source. Therefore, by using UV-Vis absorption spectroscopy, g-C_3N_4, g-C_3N_4-AgBr, and g-C_3N_4-AgI were characterized in the wavelength range from 200 to 800 nm to investigate the best absorption wavelengths. UV-Vis absorption spectra (Figure 3A) illustrates that g-C_3N_4, g-C_3N_4-AgBr, and g-C_3N_4-AgI have a strong absorption peak in this wavelength range so that a visible-light source can be useful for their excitation, revealing their proper potential to be applied as a substrate for photoelectrochemistry. Accordingly, a commercial white-light from Xe Lamp can be used as an effective light source to excite the relevant ITO electrodes modified with g-C_3N_4 / or g-C_3N_4-AgBr and g-C_3N_4-AgI, indicating the feasibility of a cheap and convenient photoelectrochemical sensor fabrication.

Electrochemical impedance spectroscopy **(**EIS) was performed to get more information about the recombination properties and electron transfer of the electrodes. The Nyquist plots for different modified electrodes, ITO/g-C_3N_4, ITO/g-C_3N_4-AgBr, and ITO/g-C_3N_4-AgI are exhibited in Figure 2B. The electron transfer resistance of the ITO/g-C_3N_4-AgI electrode is the lowest compared with those observed for others, indicating that this electrode has the highest electron conductivity. Thus, the ITO/g-C_3N_4-AgI photoelectrode has the higher ability to accelerate electron transport and increase the separation efficiency of photo-induced electrons and holes.

Fluorescence (FL) emission spectra of the g-C_3N_4, g-C_3N_4-AgBr, and g-C_3N_4-AgI nanosheets were also studied under excitation wavelengths from 250 nm to 420 nm. The main FL emission peaks for g-C_3N_4, g-C_3N_4-AgBr, and g-C_3N_4-AgI were recorded at 442, 446, and 446 nm, respectively (Figure S1 in the Supplementary Information), and these intense peaks were obtained with the excitation wavelengths at 390, 378, and 365 nm, respectively.

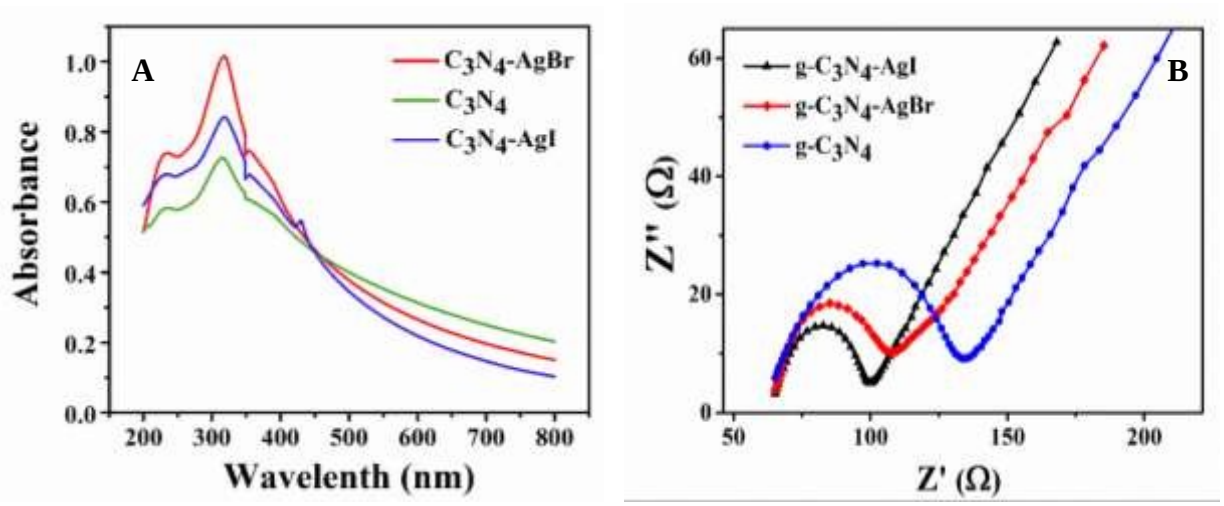

Figure 2. (A) UV−Vis absorption spectra of the as-prepared g-C_3N_4, g-C_3N_4-AgBr, and g-C_3N_4-AgI. **(B)** Nyquist plots of C_3N_4, C_3N_4-AgBr, and C_3N_4-AgI modified ITO electrodes recorded in PBS (0.1M, pH 7.4) solution.

PEC Performance of the Nanocomposites

To compare with ITO/g-C_3N_4 electrode (scheme 1A), sensitive and stable photoelectrodes based on visible-light-active g-C_3N_4-AgX (X = Br, I) nanocomposites were also fabricated on the ITO electrodes. After the irradiation of photoelectrodes with visible light, the g-C_3N_4 and AgX nanoparticles in the synthesized nanocomposites on the surface of the modified electrodes absorbed photons to generate excited electron and hole pairs, as shown in scheme 1B. Based on the band gap energy positions, the reported conduction band (CB) and valence band (VB) edge potentials for g-C_3N_4 are -1.12 eV and +1.57 eV, for AgBr are 0 eV and +2.6

View Article Online
DOI: 10.1039/C8TB01067F

eV, and for AgI are -0.15 eV and 2.95 eV, respectively. [16] So, on the basis of above information, the CB and VB energy level of g-C_3N_4 are more negative than those for AgBr and AgI, and thus helps to easily transfer of the photogenerated electrons from CB of g-C_3N_4 to the CB layer of AgBr or AgI nanoparticles and vice versa, accelerate the migration of the generated holes in the VB of AgBr or AgI nanoparticles to the VB of g-C_3N_4, which can be beneficial for desirable photoexcited electron–hole pairs separation leading to electrons and holes recombination decrease, as schematically represented in scheme 1B. Owing to the low energy level related to the CB of ITO, the generated electron can easily transfer to the ITO surface to produce photocurrent.

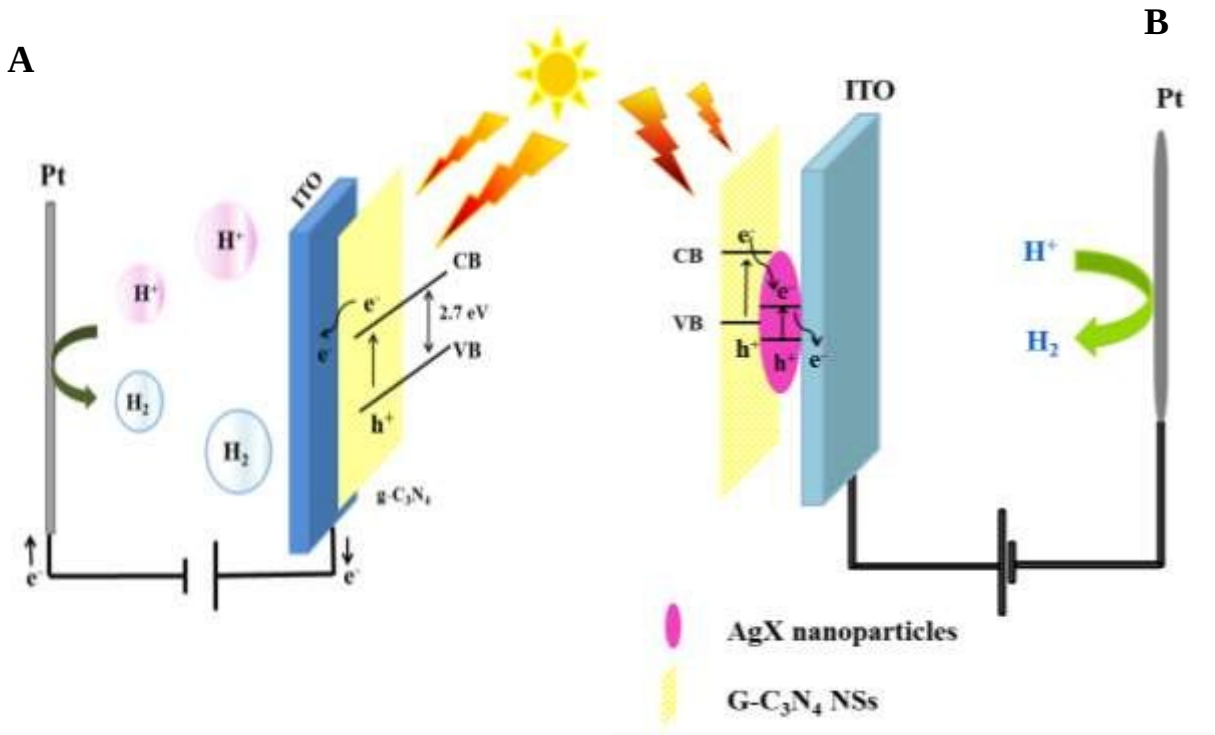

Scheme 1. (A) Schematic illustration of working principle of ITO/g-C_3N_4 electrode. **(B)** Illustration of trapping mechanism by AgX nanoparticles in the structure of g-C_3N_4.

Electron donor effect on PEC responses of ITO/g-C_3N_4, ITO/g-C_3N_4-AgBr, and ITO/g-C_3N_4-AgI electrodes

One of the noticeable roles of the addition of a proper electron donor substance to the electrolyte (phosphate buffer) solution is cleaning the holes and reducing the electron−hole recombination, leading to the photocurrent enhancement. Moreover, the scavenging of holes can prevent the photo corrosion of the as-synthesized g-C_3N_4-AgI modified photoelectrodes, hence a nontoxic and efficient electron donor will enhance the photocurrent intensity.

Effect of electron donor substance (potassium ferrocyanide) on the enhancement of photocurrent was clearly illustrates in scheme 2. One can see from scheme 2A that by adding potassium ferrocyanide as an electron donor, the generated holes in the matrix can oxidize the Fe^{2+} to Fe^{3+} and subsequently increases the photocurrent significantly. The effect of electron donor on the enhancement of the photocurrent is shown in scheme 2B. So in this work, the photocurrent was enhanced as the potassium ferrocyanide concentration was increased into the electrolyte solution up to 0.1 M, and then a constant and stable anodic photocurrent was observed.

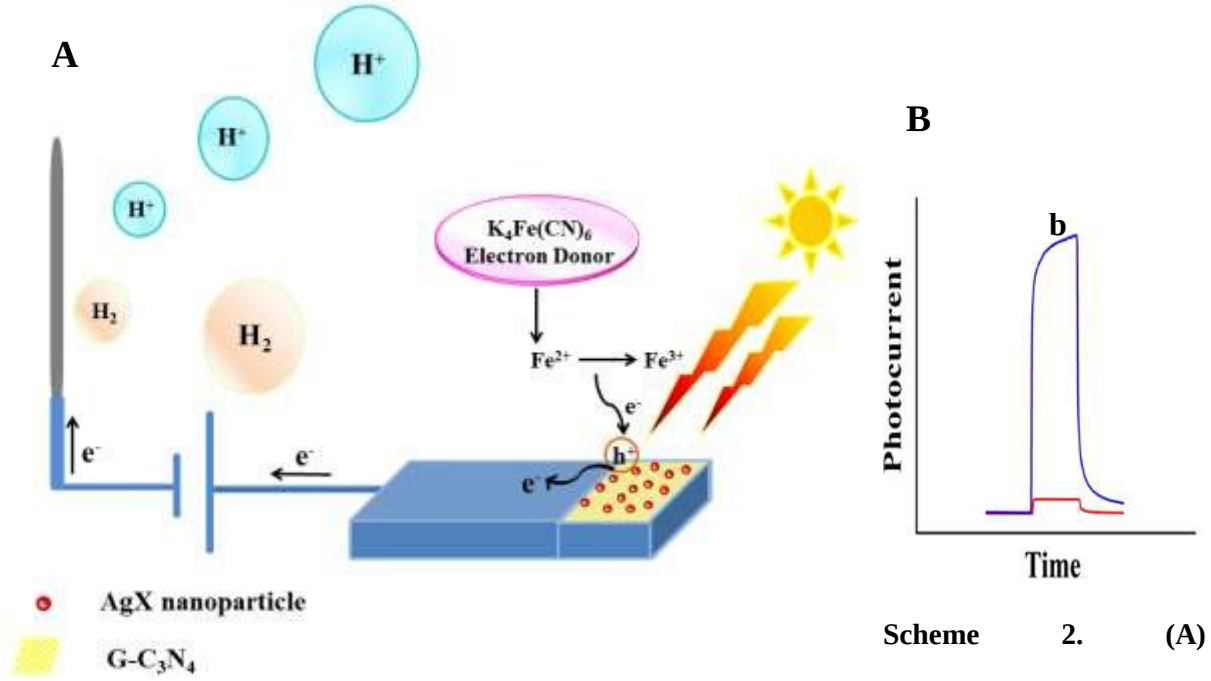

Scheme 2. (A) Photogenerated electron-hole transfer mechanism of C_3N_4-AgX in the presence of 0.1 M $K_4[Fe(CN)_6]$ and **(B)** its corresponding photocurrent in the **(a)** absence and **(b)** presence of 0.1 M $K_4[Fe(CN)_6]$.

View Article Online
DOI: 10.1039/C8TB01067F

Investigation of Applied Potential

Applied potential is one of the major parameters that is responsive for photocurrent responses and PEC detection sensitivity and selectivity. Figure 3A, B and C shows the considerable effects of applied potentials on the photocurrent responses of the as-prepared photoelectrodes in both the absence (curve a) and presence (curve b) of $K_4[Fe(CN)_6]$ (0.1 M, pH 7.0). When increasing the potential from -0.6 V to 0.2 V in PBS (curve a), a small corresponding decrease in the photocurrent of the modified electrodes can be observed. Upon addition of $K_4[Fe(CN)_6]$ (curve b), the photocurrent is almost constant between -0.6 V and -0.2 V, and then it decreases dramatically. Accordingly, -0.2 V *vs*. saturated calomel electrode (SCE) was chosen as an optimal potential to continue the PEC experiments by using ITO/g-C_3N_4, ITO/g-C_3N_4-AgBr, and ITO/g-C_3N_4-AgI electrodes.

Figure 3A', B' and C' shows the visible light effect on the stability of photocurrent responses of the fabricated electrodes based on ITO/g-C_3N_4 (A'), ITO/g-C_3N_4-AgBr (B'), and ITO/g-C_3N_4-AgI (C'). The photocurrents were measured as time (second) *vs*. photocurrent (ampere), under a potential of -0.2 V in 0.1 M PBS (pH 7.4), in the absence (curve a) and presence (curve b) of 0.1 M $K_4[Fe(CN)_6]$.

To investigate the stability and reproducibility of the photocurrent responses of the ITO/g-C_3N_4, ITO/g-C_3N_4-AgBr, and ITO/g-C_3N_4-AgI electrodes at repeated on/off cycles of the simulated visible light illumination, the photocurrents were measured for 500 seconds. In the absence and presence of $K_4[Fe(CN)_6]$, ITO/g-C_3N_4 electrode shows a stable and reproducible photocurrent responses, ITO/g-C_3N_4-AgBr electrode shows a gradual decrease in the photocurrent responses regarding to the slow decomposition of AgBr under the visible light excitation, and ITO/g-C_3N_4-AgI electrode shows a high stability and reproducibility in the photocurrent responses. Figure 3A', B' and C' clearly illustrates the significant effect of $K_4[Fe(CN)_6]$ in the buffer solution, as $K_4[Fe(CN)_6]$ can increase the photocurrents by almost

12 times for ITO/g-C_3N_4 , 4 times for ITO/g-C_3N_4-AgBr, and 6 times for ITO/g-C_3N_4-AgI. The capability of both AgBr and AgI nanoparticles for improving the photocatalytic properties of g-C_3N_4 was demonstrated in Figure 3D and as it can be seen, AgBr nanoparticles increased the photocurrent of ITO/g-C_3N_4 electrode almost 14 times, while AgI nanoparticles improved it up to 50 times. Accordingly, AgI nanoparticles may also enhance the sensitivity of this biosensing as well.

Based on the results summarized in Figure 3D, E and S5 of the Supplementary information, C_3N_4-AgI was selected as the most promising modifier for the ITO electrode and employed as a suitable photoactive matrix for the fabrication of label-free photoelectrochemical aptamer based cytosensor.

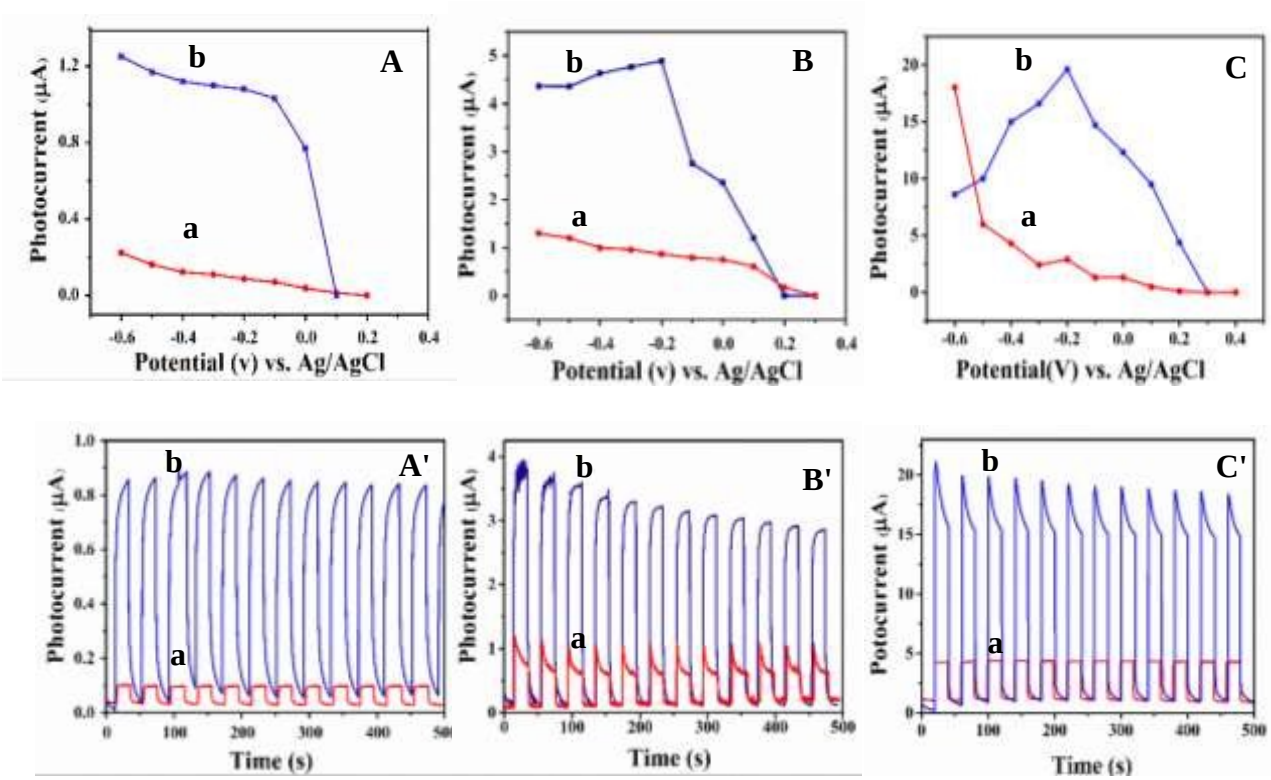

View Article Online
DOI: 10.1039/C8TB01067F

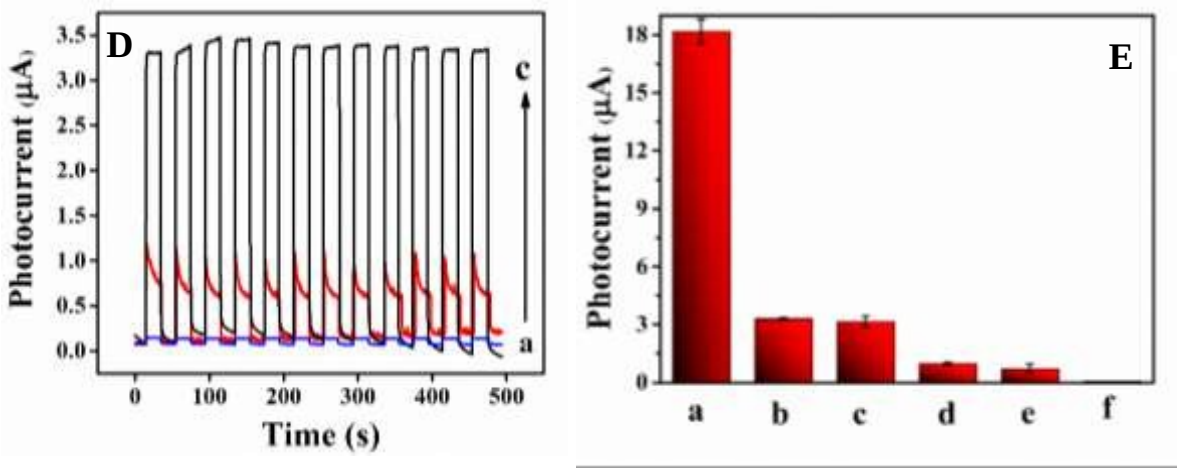

Figure 3. Applied potential effects on the photocurrent responses of the **(A)** ITO/g-C_3N_4, **(B)** ITO/g-C_3N_4-AgBr**,** and **(C)** ITO/g-C_3N_4-AgI electrodes and **(A'**, **B'** and **C')** time-based photocurrent responses in the potential of -0.2 V for the mentioned electrodes respectively in PBS (0.1 M, pH 7.4) in the **(a)** absence and **(b)** presence of 0.1 M $K_4[Fe(CN)_6]$ with visible light excitation. **(D)** Time based Photocurrent comparison of 3 different photoelectrodes **(a)** ITO/C_3N_4**, (b)** ITO/C_3N_4-AgBr and **(c)** ITO/C_3N_4-AgI in PBS (0.1 M, pH 7.4). **(E)** Peak height of the photocurrents of 3 different photoelectrodes **(a, b)** ITO/C_3N_4-AgI, **(c, d)** ITO/C_3N_4-AgBr and **(e, f)** ITO/C_3N_4 in buffer solution in the presence and absence of $K_4[Fe(CN)_6]$.

Construction of PEC Aptamer based cytosensor

As can be seen from scheme 3 (a, b and c) for construction of PEC cytosensor, different materials were used to modify the electrode surface. Accordingly, the interface properties of different stages of the biosensor fabrication such as ITO, ITO/C_3N_4-AgI, ITO/C_3N_4-AgI/Aptamer, and ITO/C_3N_4-AgI/Aptamer/Hela cells were characterized by means of EIS, cyclic voltammetry (CV), and PEC methods. During every construction step of the biosensor each potential electrode was analyzed by using EIS in the frequency range from 0.01–100 kHz at potential of 20 mV in KCl (0.1 M) solution containing a redox probe of 5 mM $K_3[Fe(CN)_6]$/ K_4 $[Fe(CN)]_6]$ (1:1) mixture. One can see from Figure 4A that bare ITO

electrode shows the electron transfer resistance (Ret) value of 23 Ω (curve a). Successful assembly of C_3N_4-AgI increased the Ret value up to 39 Ω (curve b) and owing to the absorption of aptamer on C_3N_4-AgI films, the Ret value of the ITO/C_3N_4-AgI /Aptamer electrode reached to 83 Ω (curve c). Finally, Hela cancer cells were bonded to the aptamers which were already immobilized on the electrode surface, and in this step the Ret value of the electrode enhanced to 188 Ω (curve d). The reason behind the Ret value increase could be attributed to the fact that the nonconductive properties of the g-C_3N_4 (as g-C_3N_4-AgI nanocomposite), ss DNA aptamer, and Hela cells can barricade the mass transport of the redox probe to the electrode surface and lessen the electron transfer rate, indicating the successful assembly of the photoactive and sensing material on the electrode surface.

Typical cyclic voltammograms of the different modified electrodes were obtained after every layer assembly of photoactive and biological species on ITO electrode, measured in PBS (0.1 M. pH 7.4) containing 5×10^{-4} M $K_3[Fe(CN)_6]$/ K_4 $[Fe(CN)]_6]$ (1:1) and 0.1 M KCl solution which are shown in Figure 4B. Owing to the higher conductivity of ITO and ITO/C_3N_4-AgI electrodes, the largest redox peaks are observed for these two electrodes before immobilizing with aptamer (curves a and b). Comparing with the bare ITO electrode (curve a), the largest peak current of ITO/C_3N_4-AgI electrode (curve b) is due to the larger surface area of ITO/C_3N_4-AgI electrode because of the presence of AgI nanoparticles and its conductive property in the structure of g-C_3N_4 NSs. After the assembly of aptamer, the photocurrent response was greatly reduced owing to the decrease in the electron transfer capability of the modified ITO/C_3N_4-AgI/Aptamer electrode (curve c). Finally, the Hela cells were immobilized with aptamer modified electrode. As it can be seen from curve d a significant decrease in the redox current was observed as a result of the hela cell-aptamer binding that consequently causes decrease in the electron transfer on the surface of modified ITO/C_3N_4-AgI/Aptamer/Hela electrode. By using photoelectrochemical measurements, the

fabrication process of the cytosensor was also monitored. The electrode modification-induced changes in the photocurrent are shown in Figure 4C. After adhering the g-C_3N_4-AgI nanosheet to the surface of a bare ITO, a significantly enhanced photocurrent intensity was observed which demonstrating that g-C_3N_4-AgI nanosheet is an ideal choice for the construction of a photoelectrochemical biosensor (curve a). Gradual decrease in photocurrent intensity after immobilization with the aptamer and Hela cells could be attributed to the fact that the immobilization of these biomaterials on the surface of ITO/g-C_3N_4-AgI electrode decreases the photoactive reaction surface of ITO/g-C_3N_4-AgI available for the interaction with light. As expected, the successive binding of the aptamer (100 nM) on the surface of the ITO/C_3N_4-AgI electrode induces significant decrease in the photocurrents (curve b). After the incubation of the obtained cytosensor with Hela cells, the photocurrent intensity further decreases (curve c). These results demonstrate the successful fabrication of a facile and label-free photoelectrochemical cytosensor for quantitative detection of Hela cells based on the ITO/g-C_3N_4-AgI electrode.

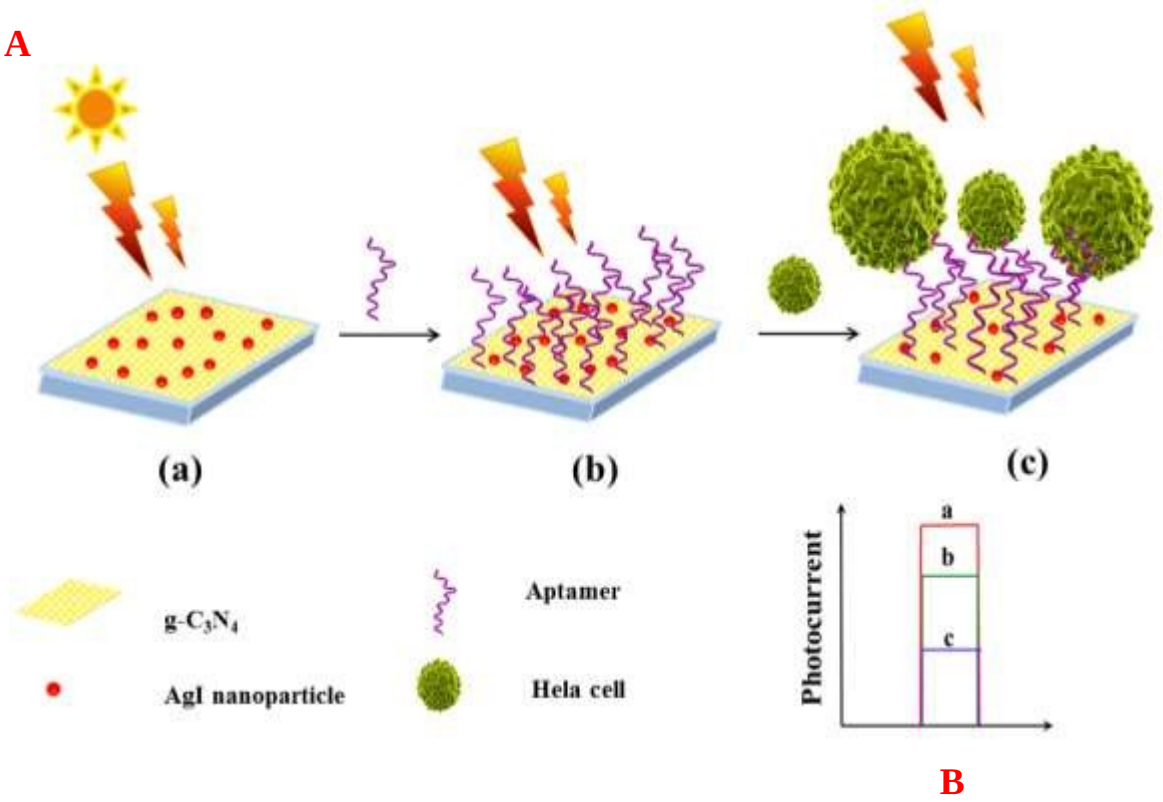

Scheme 3. Schematic illustration of PEC Cytosensor fabrication process (a, b and c) **(A)** and its corresponding photocurrents **(B)**.

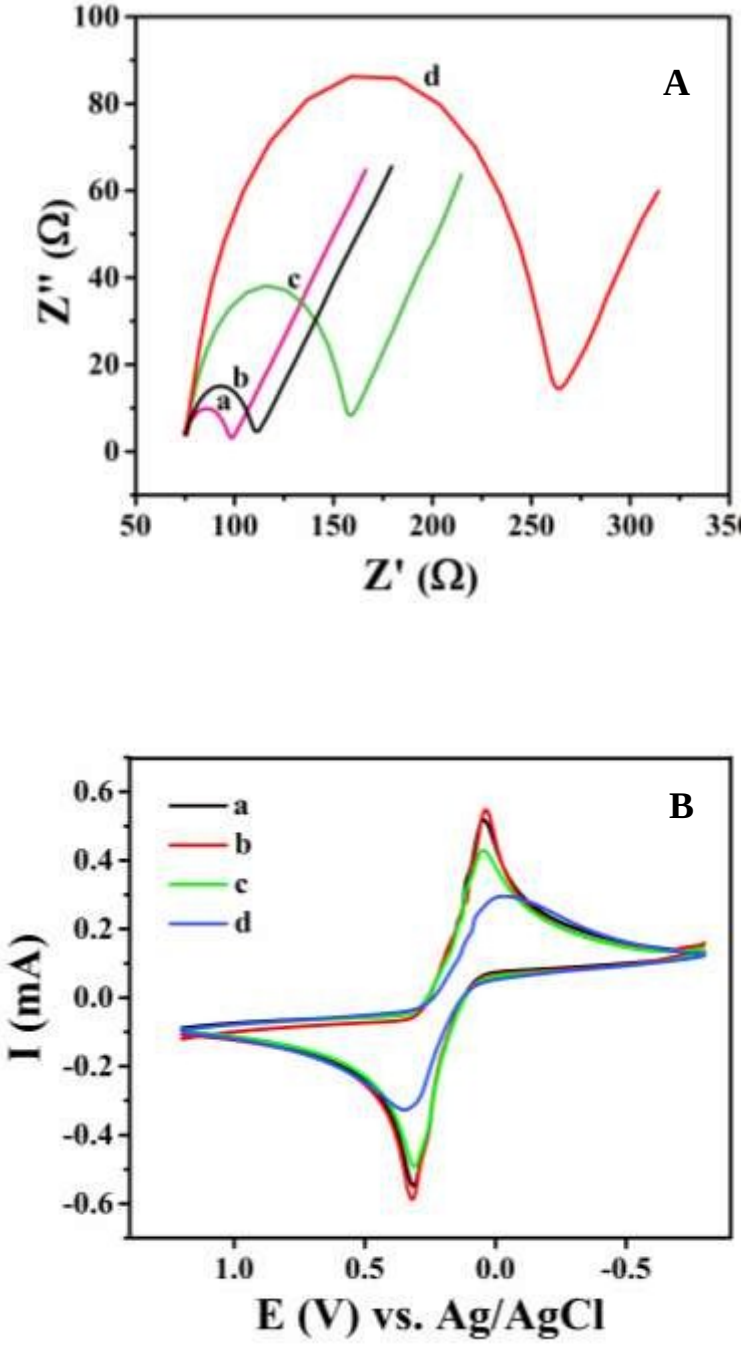

View Article Online
DOI: 10.1039/C8TB01067F

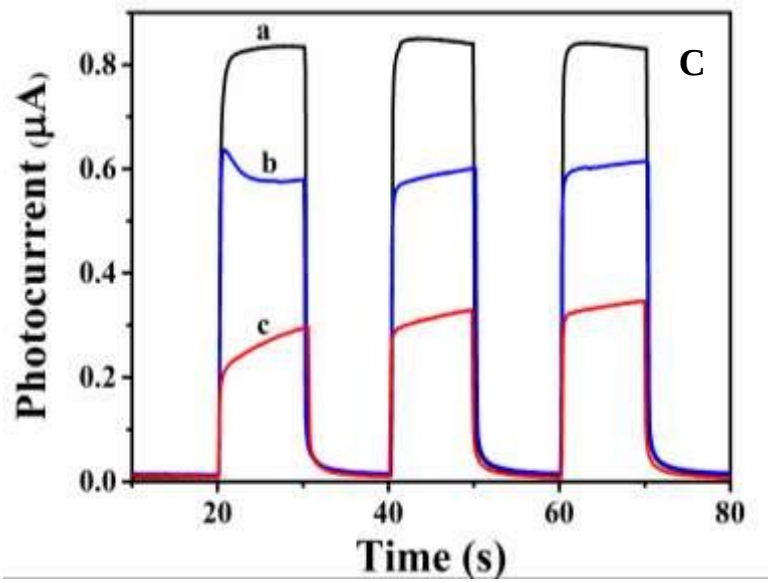

Figure 4. (A) Nyquist plots of EIS and **(B)** CV at a scan rate of 100 mV s^{-1} in PBS (0.1 M. pH 7.4) containing 5×10^{-4} M $K_3[Fe(CN)_6]$/ K_4 $[Fe(CN)]_6$] (1:1) and 0.1 M KCl for different modification steps of layer-by-layer assembled electrode on the ITO surface **(a-d); (a)** ITO, **(b)** ITO/C_3N_4-AgI, **(c)** ITO/C_3N_4-AgI /Aptamer and **(d)** ITO/C_3N_4-AgI/ Aptamer /Hela. **(C)** Photocurrent response of ITO/C_3N_4-AgI **(a)**, ITO/C_3N_4-AgI /Aptamer **(b)**, and ITO/C_3N_4-AgI/ Aptamer /Hela **(c)** in PBS (0.1 M. pH 7.4)**.**

Analytical Performances of the cytosensor

The efficiency of this label-free photoelectrochemical cytosensor and its reproducibility and stability for the detection of Hela cells were further exploited. The PEC Cytosensor fabrication process and its corresponding photocurrent was illustrated in scheme 3, where the resulted photocurrent intensity was related directly to the binding affinity between the immobilized aptamers and the target cells. As shown in Figures 5A and Figure S6 in the Supplementary information, our observations of the EIS measurements demonstrate a good specific binding of aptamer with Hela cells and also negligible effect of the electrode surface absorption, where a considerable decrease in the photocurrent could be observed upon addition of Hela cells. It is noted that the increased number of Hella cells reacted with the

aptamers could readily lead to a significant suppression of the photocurrent. Furthermore, it can be observed from Figure 5B that the decrease in the photocurrent has a linear relation with the logarithm of different concentration of Hela cells ranging from 10 to 1×10^6 cells/mL, the equation of which was photocurrent ($*10^{-7}$) = 0.4933 + 1.1686 log [cell density] (R = 0.9751). The detection limit was calculated as 5 cells/mL (S/N = 3), according to three times measurement of the blank signal for calculating the standard deviation (PEC signal which was obtained when this biosensor already incubated with aptamer was treated in fresh culture medium without cells). The analytical performance of this cytosensor was compared to the previously reported cytosensors for the detection of the Hela cells with different methods, as shown in table S2 of the Supplementary information. Our results also present a favorable examination of the Hela cells with a large detection range and a comparable detection limit with the help of sga16 and the PEC interface. The results indicate that our designed PEC cytosensor is very promising for applications in the cancer cell detection and exhibits an excellent selectivity for the Hela cells.

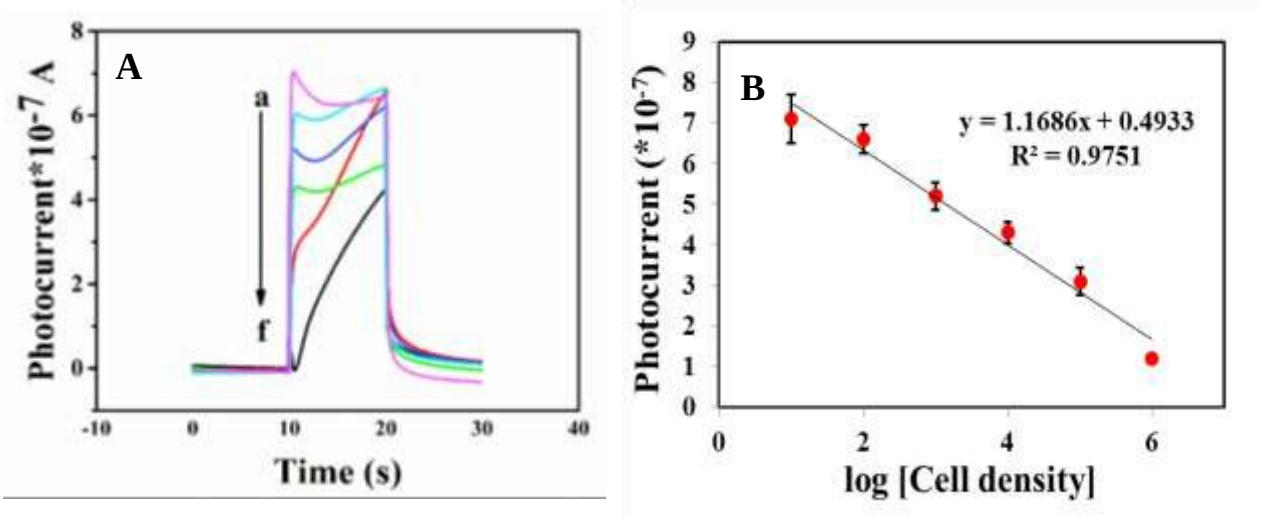

Figure 5. (A) Photocurrent responses of ITO/C_3N_4-AgI/Aptamer after incubating with various concentrations of the Hela cells **(a)** 10, **(b)** 1×10^2, **(c)** 1×10^3, **(d)** 1×10^4, **(e)** 1×10^5, **(f)** 1×10^6 in PBS (0.1 M, pH 7.4). **(B)** Calibration curve of the cytosensor for Hela cells detection; corresponding

View Article Online
DOI: 10.1039/C8TB01067F

data points and error bars is related to the average and standard deviations from four individual experiments.

Control Experiments

The presented cytosensor also exhibited an excellent selectivity for the detection of Hela cells, as confirmed by EIS and PEC studies. The comparison of obtained analytical signals from the sensor for Hela cells through EIS and PEC measurements with four control human cancer and disease cells, including breast cancer cell (MCF-7), lung carcinoma (A549), human caucasian burkitt's lymphoma (Ramos), and human promyelocytic leukemia cells (HL60) shows that when these control cells at the same concentration as Hela cells, i.e., 1×10^5 cells/mL cells were incubated with the CEM/PTK7 aptamer on the modified electrode surface, only small Ret and PEC changes (signal change < 0.5%) were observed compared with the Hela cells immobilized with CEM/PTK7 aptamer, indicating the lack of immobilization of the control cells with CEM/PTK7 aptamer and the high selectivity of the sensor toward Hela cells. Accordingly, the results of these studies introduced a reasonable and reliable application of the fabricated cytosensor for high-sensitive diagnosis of Hela cancer cells. The Influences of some common inorganic ions and biological compounds interferences on the designed biosensor were evaluated and these results were summarized in Table S3.

4. Conclusion

In summary, a facile label-free PEC cytosensor was developed in this study by using g-C_3N_4 NSs doped with AgI NPs with an approximate average size of 70 nm. Because of the significant role of AgI NPs on the g-C_3N_4 NSs structure, g-C_3N_4-AgI NSs exhibited intense and stable PEC current in comparison with g-C_3N_4 NSs. Since one of the major challenges in the scope of biosensors and biomedical engineering is a sensitive detection of cervical cancer cells, an accurate and selective biosensor is designed for detecting the related cancer cells by

View Article Online
DOI: 10.1039/C8TB01067F

using fabricated aptamer-based photoelectrochemical cytosensors. In addition, the high-affinity and specific interactions between aptamer sga16 (anti-CEM/PTK7) toward the Hela cells effectively improved the sensitivity and the selectivity of the relevant cancer cell detection when applied at the surface of the photoelectrochemical electrode as the recognition layer. Moreover, along with the low overpotential and good reproducibility, stability, and specificity, the designed photoelectrochemical cytosensor can determined Hela cells at the concentrations as low as 5 cells/mL with a linear relationship between photocurrent and the logarithmic value of cells concentration, which was found in the range of 10 to 1.0×10^6 cells/ml with a low detection limit and correlation coefficient of 0.9751. In addition, simple fabrication, selective and label-free properties of the as-prepared photoelectrochemical biosensor made it a reliable bioanalysis tool for the Hela cells detection. To compare with the previously reported biosensors for Hella cells diagnosis with different methods this facile PEC cytosensor exhibits excellent efficiency that could find promising applications in related biomedical field.

View Article Online
DOI: 10.1039/C8TB01067F

ACKNOWLEDGMENTS

This work was supported financially by the National Natural Science Foundation of China (91753106, 21675023, 81325011, 21327902), the National High Technology Research & Development Program of China (2017YFA0205300, 2015AA020502) and primary research and development plan of Jiangsu province (modern agriculture) (BE2017317).

Conflict of Interest

R. Motaghed Mazhabi, L. Ge, H. Jiang and X. Wang declare that they have no conflict of interest.

Ethical approval: All procedures performed in studies were in accordance with the ethical standards of the institutional and/or national research committee and with the 1964 Helsinki declaration and its later amendments or comparable ethical standards.

View Article Online
DOI: 10.1039/C8TB01067F

Notes and references

1. N. Savage, *Nature*, 2011, **471**, S14-S15.
2. T. Yu, P.-P. Dai, J.-J. Xu and H.-Y. Chen, *ACS Appl. Mater. Interfaces*, 2016, **8**, 4434-4441.
3. Z. Han and Z.-R. Lu, *J. Mater. Chem. B*, 2017, **5**, 639-654.
4. X. Zhang, K. Xiao, L. Cheng, H. Chen, B. Liu, S. Zhang and J. Kong, *Anal. Chem.*, 2014, **86**, 5567-5572.
5. J. A. Phillips, Y. Xu, Z. Xia, Z. H. Fan and W. Tan, *Anal. Chem.*, 2009, **81**, 1033-1039.
6. S. K. Singh, C. Hawkins, I. D. Clarke, J. A. Squire, J. Bayani, T. Hide, R. M. Henkelman, M. D. Cusimano and P. B. Dirks, *Nature*, 2004, **432**, 396-401.
7. D. Schamhart, J. Swinnen, K. H. Kurth, A. Westerhof, R. Kusters, H. Borchers and C. Sternberg, *Clin. Chem.*, 2003, **49**, 1458-1466.
8. V. Gubala, L. F. Harris, A. J. Ricco, M. X. Tan and D. E. Williams, *Anal. Chem.*, 2012, **84**, 487-515.
9. K. Yan, Y. Liu, Y. H. Yang and J. D. Zhang, *Anal. Chem.*, 2015, **87**, 12215-12220.
10. Y.-C. Zhu, N. Zhang, Y.-F. Ruan, W.-W. Zhao, J.-J. Xu and H.-Y. Chen, *Anal. Chem.*, 2016, **88**, 5626-5630.
11. W.-W. Zhao, J.-J. Xu and H.-Y. Chen, *Chem. Soc. Rev.*, 2015, **44**, 729-741.
12. L. Li, Y. Zhang, L. Zhang, S. Ge, H. Liu, N. Ren, M. Yan and J. Yu, *Anal. Chem.*, 2016, **88**, 5369-5377.
13. Y. An, Y. Fu, D. Lu, Y. Wang, W. Bi, Z. Xu, S. Dong, S. Zhang, C. Wang and W. Zhang, *J. Mater. Chem. B*, 2014, **2**, 1644-1652.
14. S. Chen, H. Nan, X. Zhang, Y. Yan, Z. Zhou, Y. Zhang and K. Wang, *J. Mater. Chem. B*, 2017, **5**, 3718-3727.

15. Z. Zhou, J. Wang, J. Yu, Y. Shen, Y. Li, A. Liu, S. Liu and Y. Zhang, *J. Am. Chem. Soc.*, 2015, **137**, 2179-2182.
16. L. Xu, J. Xia, H. Xu, J. Qian, J. Yan, L. Wang, K. Wang and H. Li, *Analyst*, 2013, **138**, 6721-6726.
17. Y. Zhang and M. Antonietti, *Chem. Asian J.*, 2010, **5**, 1307-1311.
18. X. Wang, K. Maeda, X. Chen, K. Takanabe, K. Domen, Y. Hou, X. Fu and M. Antonietti, *J. Am. Chem. Soc.*, 2009, **131**, 1680-1681.
19. E. Z. Lee, Y.-S. Jun, W. H. Hong, A. Thomas and M. M. Jin, *Angew. Chem. Int. Ed.*, 2010, **49**, 9706-9710.
20. E. Z. Lee, S. U. Lee, N.-S. Heo, G. D. Stucky, Y.-S. Jun and W. H. Hong, *Chem. Commun.*, 2012, **48**, 3942-3944.
21. X. Wang, K. Maeda, A. Thomas, K. Takanabe, G. Xin, J. M. Carlsson, K. Domen and M. Antonietti, *Nat. Mater.*, 2009, **8**, 76-80.
22. F. Goettmann, A. Thomas and M. Antonietti, *Angew. Chem. Int. Ed.*, 2007, **46**, 2717-2720.
23. F. Su, S. C. Mathew, G. Lipner, X. Fu, M. Antonietti, S. Blechert and X. Wang, *J. Am. Chem. Soc.*, 2010, **132**, 16299-16301.
24. S. C. Yan, Z. S. Li and Z. G. Zou, *Langmuir*, 2009, **25**, 10397-10401.
25. X. Wang, X. Chen, A. Thomas, X. Fu and M. Antonietti, *Adv. Mater.*, 2009, **21**, 1609-+.
26. X. Zhang, X. Xie, H. Wang, J. Zhang, B. Pan and Y. Xie, *J. Am. Chem. Soc.*, 2013, **135**, 18-21.
27. L. Chen, X. Zeng, P. Si, Y. Chen, Y. Chi, D.-H. Kim and G. Chen, *Anal. Chem.*, 2014, **86**, 4188-4195.
28. Y. Zhang, M. Yan, S. Ge, C. Ma, J. Yu and X. Song, *J. Mater. Chem. B*, 2016, **4**, 4980-4987.

29. J.-X. Sun, Y.-P. Yuan, L.-G. Qiu, X. Jiang, A.-J. Xie, Y.-H. Shen and J.-F. Zhu, *Dalton Trans.*, 2012, **41**, 6756-6763.
30. Y. Zang, R. Farnood and J. Currie, *Chem. Eng. Sci.*, 2009, **64**, 2881-2886.
31. H. Xu, J. Yan, Y. Xu, Y. Song, H. Li, J. Xia, C. Huang and H. Wan, *Appl. Catal., B*, 2013, **129**, 182-193.
32. M. Abou Asi, C. He, M. Su, D. Xia, L. Lin, H. Deng, Y. Xiong, R. Qiu and X.-z. Li, *Catal. Today*, 2011, **175**, 256-263.
33. C. Wu, L. Shen, Y. C. Zhang and Q. Huang, *Mater. Lett.*, 2012, **66**, 83-85.
34. J. Cao, B. Luo, H. Lin and S. Chen, *J. Hazard. Mater.*, 2011, **190**, 700-706.
35. H. Xu, Y. Xu, H. Li, J. Xia, J. Xiong, S. Yin, C. Huang and H. Wan, *Dalton Trans.*, 2012, **41**, 3387-3394.
36. J.-F. Guo, B. Ma, A. Yin, K. Fan and W.-L. Dai, *Appl. Catal., B*, 2011, **101**, 580-586.
37. Y. Bi, S. Ouyang, J. Cao and J. Ye, *Phys. Chem. Chem. Phys.*, 2011, **13**, 10071-10075.
38. J. Cao, B. Luo, H. Lin and S. Chen, *J. Mol. Catal. A: Chem.*, 2011, **344**, 138-144.
39. Y. Sun, H. Cheng, S. Gao, Z. Sun, Q. Liu, Q. Liu, F. Lei, T. Yao, J. He, S. Wei and Y. Xie, *Angew. Chem. Int. Ed.*, 2012, **51**, 8727-8731.
40. R. Li, Y. Liu, L. Cheng, C. Yang and J. Zhang, *Anal. Chem.*, 2014, **86**, 9372-9375.
41. Y. Liu, R. Wang, Y. Zhu, R. Li and J. Zhang, *Sens. Actuators, B*, 2015, **210**, 355-361.
42. R. Wang, K. Yan, F. Wang and J. Zhang, *Electrochim. Acta*, 2014, **121**, 102-108.
43. N. Haddour, J. Chauvin, C. Gondran and S. Cosnier, *J. Am. Chem. Soc.*, 2006, **128**, 9693-9698.
44. J. J. Yang, P. C. Gao, Y. X. Liu, R. X. Li, H. M. Ma, B. Du and Q. Wei, *Biosens. Bioelectron.*, 2015, **64**, 13-18.
45. M. Zheng, Y. Cui, X. Li, S. Liu and Z. Tang, *J. Electroanal. Chem.*, 2011, **656**, 167-173.
46. X. Zhang, Y. Zhao, S. Li and S. Zhang, *Chem. Commun.*, 2010, **46**, 9173-9175.

47. X. Cong, G.-C. Fan, X. Wang, E. S. Abdel-Halim and J.-J. Zhu, J. Mater. Chem. B, 2016, **4**, 6117-6124.

48. Y. Liu, N. Tuleouva, E. Ramanculov and A. Revzin, *Anal. Chem.*, 2010, **82**, 8131-8136.

49. B. R. Baker, R. Y. Lai, M. S. Wood, E. H. Doctor, A. J. Heeger and K. W. Plaxco, *J. Am. Chem. Soc.*, 2006, **128**, 3138-3139.

50. S. Tombelli, M. Minunni and M. Mascini, *Biosens. Bioelectron.*, 2005, **20**, 2424-2434.

51. I. German, D. D. Buchanan and R. T. Kennedy, *Anal. Chem.*, 1998, **70**, 4540-4545.

52. W. Tan, M. J. Donovan and J. Jiang, *Chem. Rev.*, 2013, **113**, 2842-2862.

53. J. Li, X. Hu, S. Shi, Y. Zhang and T. Yao, *J. Mater. Chem. B*, 2016, **4**, 1361-1367.

54. K.-M. Song, M. Cho, H. Jo, K. Min, S. H. Jeon, T. Kim, M. S. Han, J. K. Ku and C. Ban, *Anal. Chem.*, 2011, **415**, 175-181.

55. X. Sun, F. Li, G. Shen, J. Huang and X. Wang, *Analyst*, 2014, **139**, 299-308.

56. X. Bai, H. Hou, B. Zhang and J. Tang, *Biosens. Bioelectron.*, 2014, **56**, 112-116.

57. X. Zeng, S. Ma, J. Bao, W. Tu and Z. Dai, *Anal. Chem.*, 2013, **85**, 11720-11724.

58. S. Nagatoishi, T. Nojima, E. Galezowska, B. Juskowiak and S. Takenaka, *ChemBioChem*, 2006, **7**, 1730-1737.

59. M. S. Yang, M. E. McGovern and M. Thompson, *Anal. Chim. Acta*, 1997, **346**, 259-275.

60. O. H. Laitinen, V. P. Hytoenen, H. R. Nordlund and M. S. Kulomaa, *Cell. Mol. Life Sci.*, 2006, **63**, 2992-3017.

61. E. Paleček and F. Jelen, *Crit. Rev. Anal. Chem.*, 2002, **32**, 261-270.

62. H. Li, Y. Mu, J. Yan, D. Cui, W. Ou, Y. Wan and S. Liu, *Anal. Chem.*, 2015, **87**, 2007-2015.

63. R. Motaghed Mazhabi, L. Ge, H. Jiang and X. Wang, *Biosens. Bioelectron.*, 2018, **107**, 54-61.

64. Y. Feng, J. Shen, Q. Cai, H. Yang and Q. Shen, *New J. Chem.*, 2015, **39**, 1132-1138.

View Article Online
DOI: 10.1039/C8TB01067F

“Table of contents”

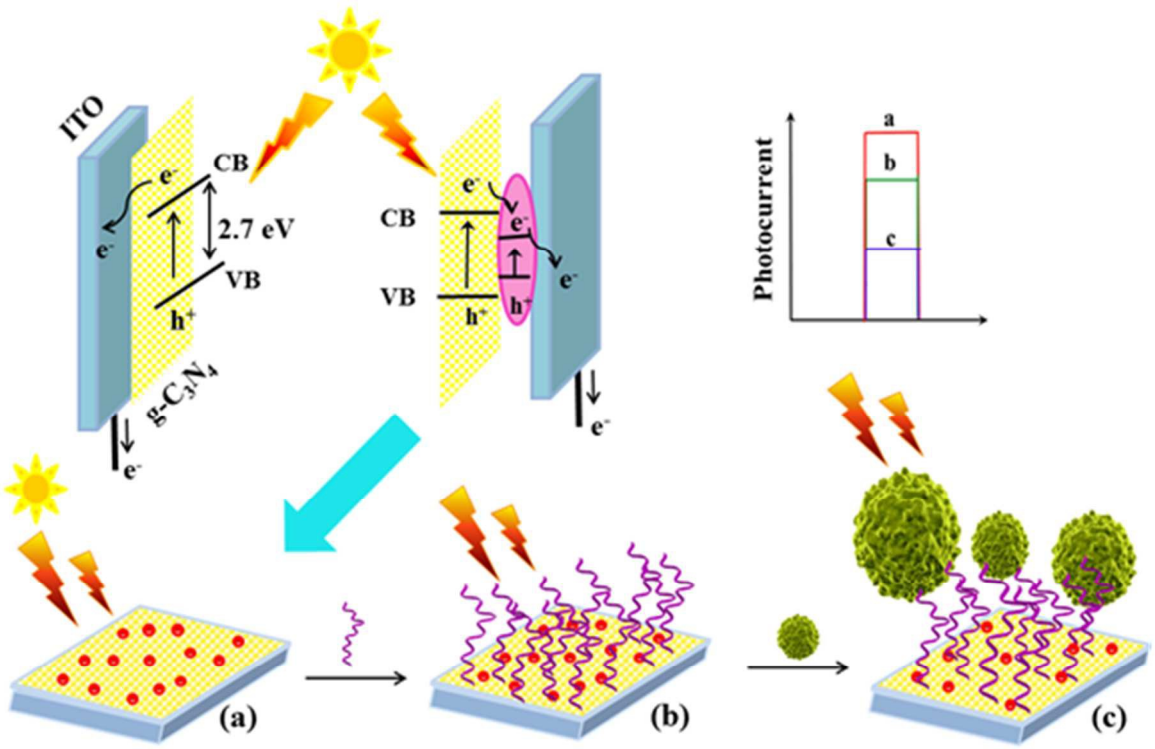

Illustration of PEC Cytosensor fabrication process and its corresponding photocurrents